A Sir2-regulated locus control region in the recombination enhancer of *Saccharomyces cerevisiae* specifies chromosome III structure

Mingguang Li[2,3], Ryan D. Fine[1,3], Manikarna Dinda[1], Stefan Bekiranov[1], and Jeffrey S. Smith[1,*]

[1]Department of Biochemistry and Molecular Genetics, University of Virginia School of Medicine, Charlottesville, VA 22908. [2]Department of Laboratory Medicine, Jilin Medical University, Jilin, 132013, China

[3]Equally contributed to the work.

[*]Corresponding Author

Department of Biochemistry and Molecular Genetics

University of Virginia School of Medicine

Pinn Hall, Box 800733

Charlottesville, VA 22908

Phone: 434-243-5864

Fax: 434-924-5069

Email: jss5y@virginia.edu

Keywords: *SIR2*, condensin, *RDT1*, Hi-C, mating-type switching, chromosome structure, yeast, *Saccharomyces cerevisiae*, yeast, donor preference

Abstract

The NAD^+-dependent histone deacetylase Sir2 was originally identified in *Saccharomyces cerevisiae* as a silencing factor for *HML* and *HMR*, the heterochromatic cassettes utilized as donor templates during mating-type switching. *MAT*a cells preferentially switch to *MAT*α using *HML* as the donor, which is driven by an adjacent *cis*-acting element called the recombination enhancer (RE). In this study we demonstrate that Sir2 and the condensin complex are recruited to the RE exclusively in *MAT*a cells, specifically to the promoter of a small gene within the right half of the RE known as *RDT1*. We go on to demonstrate that the *RDT1* promoter functions as a locus control region (LCR) that regulates both transcription and long-range chromatin interactions. Sir2 represses the transcription of *RDT1* until it is redistributed to a dsDNA break at the MAT locus induced by the HO endonuclease during mating-type switching. Condensin is also recruited to the *RDT1* promoter and is displaced upon HO induction, but does not significantly repress *RDT1* transcription. Instead condensin appears to promote mating-type switching efficiency and donor preference by maintaining proper chromosome III architecture, which is defined by the interaction of *HML* with the right arm of chromosome III, including *MAT*a and *HMR*. Remarkably, eliminating Sir2 and condensin recruitment to the *RDT1* promoter disrupts this structure and reveals an aberrant interaction between *MAT*a and *HMR*, consistent with the partially defective donor preference for this mutant. Global condensin subunit depletion also impairs mating type switching efficiency and donor preference, suggesting that modulation of chromosome architecture plays a significant role in controlling mating type switching, thus providing a novel model for dissecting condensin function *in vivo*.

Author summary

Sir2 is a highly conserved NAD^+-dependent protein deacetylase and defining member of the sirtuin protein family. It was identified about 40 years ago in the budding yeast, *Saccharomyces cerevisiae*, as a gene required for silencing of the cryptic mating-type loci, *HML* and *HMR*. These heterochromatic cassettes are utilized as templates for mating-type switching, whereby a programmed DNA double-strand break at the *MAT*a or *MAT*α locus is repaired by gene conversion to the opposite mating type. The preference for switching to the opposite mating type is called donor preference, and in *MAT*a cells, is driven by a cis-acting DNA element called the recombination enhancer (RE). It was believed that the only role for Sir2 in mating-type switching was silencing HML and HMR. However, in this study we show that Sir2 also regulates expression of a small gene (RDT1) in the RE that is activated during mating-type switching. The promoter of this gene is also bound by the condensin complex, and deleting this region of the RE drastically changes chromosome III structure and alters donor preference. The RE therefore appears to function as a complex locus control region (LCR) that links transcriptional control to chromatin architecture, and thus provides a new model for investigating the underlying mechanistic principles of programmed chromosome architectural dynamics.

Introduction

Since the first descriptions of mating-type switching in budding yeast approximately 40 years ago, characterization of this process has led to numerous advances in understanding mechanisms of gene silencing (heterochromatin), cell-fate determination (mating-type), and homologous recombination (reviewed in [1]. For example, the NAD^+-dependent histone deacetylase, Sir2, and other Silent Information Regulator (SIR) proteins, were genetically identified due to their roles in silencing the heterochromatic *HML* and *HMR* loci, which are maintained as silenced copies of the active *MAT*α and *MAT*a loci, respectively [2-4]. The SIR silencing complex (Sir2-Sir3-Sir4) is recruited to cis-acting E and I silencer elements flanking *HML* and *HMR* through physical interactions with silencer binding factors Rap1, ORC, and Abf1, as well as histones H3 and H4 (reviewed in [5]).

HML and *HMR* play a critical role in mating-type switching. Haploid cells of the same mating-type cannot mate to form diploids, the preferred cell type in the wild. Therefore, in order to facilitate mating and diploid formation, haploid mother cells switch their mating type by expressing HO endonuclease, which introduces a programmed DNA double-strand break (DSB) at the *MAT* locus [6]. The break is then repaired by homologous recombination using either *HML* or *HMR* as a donor template for gene conversion [6, 7]. This change in mating type enables immediate diploid formation between mother and daughter. *HO* is deleted from most standard lab strains in order to maintain them as haploids, so expression of *HO* from an inducible promoter such as P_{GAL1} is commonly used to switch mating types during strain construction [8].

There is a "donor preference" directionality to mating-type switching such that ~90% of the time, the HO-induced DSB is repaired to the opposite mating type [9]. For example, *MAT*α cells preferentially switch to *MAT*a using *HMR* as the donor. However, while both silent mating

loci can be utilized as a donor template, usage of *HML* by *MAT*a cells requires a 2.5 kb intergenic region located ~17 kb from *HML* called the recombination enhancer (RE) [10]. Donor preference activity within the RE has been further narrowed down to a 700 bp segment containing an Mcm1/α2 binding site (DPS1) and multiple Fkh1 binding sites [10]. The RE is active in *MAT*a cells, requiring Mcm1 and Fkh1 activity at their respective binding sites [10-12]. The RE is inactivated in *MAT*α cells due to expression of transcription factor α2 from *MAT*α [13], which forms a repressive heterodimer with Mcm1 (Mcm1/α2) to repress *MAT*a-specific genes [1]. Current models for donor preference posit that Fkh1 at the RE helps position *HML* in close proximity with *MAT*a by interacting with threonine-phosphorylated H2A (γ-H2AX) and Mph1 DNA helicase at the HO-induced DNA DSB [14, 15].

Sir2-dependent silencing of *HML* and *HMR* has two known functions related to mating-type switching. First, *HML* and *HMR* must be silenced in haploids to prevent formation of the a1/α2 heterodimer, which would otherwise inactivate haploid-specific genes such as *HO* [16]. Second, heterochromatin structure at *HML* and *HMR* blocks cleavage by HO, thus restricting its activity to the fully accessible *MAT* locus [17, 18]. Here we describe new roles for Sir2 and the condensin complex within the RE during mating-type switching. ChIP-seq analysis revealed strong overlapping binding sites for Sir2 and condensin at the promoter of a small gene within the RE known as *RDT1*. Sir2 was found to repress the *MAT*a-specific transcription of *RDT1*, which is also translated into a small 28 amino acid peptide. *RDT1* expression is also dramatically upregulated during mating-type switching when Sir2 redistributes to the HO-induced DNA DSB at *MAT*a. Furthermore, eliminating Sir2/condensin recruitment to the *RDT1* promoter disrupts chromosome III architecture such that mating-type switching efficiency and donor preference are partially impaired. The *RDT1* promoter region therefore functions like a classic locus control

region (LCR) in *MAT*a yeast cells, regulating localized transcription as well as long-range chromosome interactions.

Results

Sir2 and condensin associate with the recombination enhancer (RE)

We previously characterized global sirtuin distribution using ChIP-Seq to identify novel loci regulated by Sir2 and its homologs [19]. Significant overlap was observed between binding sites for Sir2, Hst1, or Sum1 with previously described condensin binding sites [19, 20], suggesting a possible functional connection. ChIP-Seq was therefore performed on WT and *sir2*Δ strains in which the condensin subunit Smc4 was C-terminally tagged (13xMyc) (Fig 1A). To avoid "hyper-ChIPable" loci that can appear in yeast ChIP-seq experiments, we also ran nuclear localized GFP controls [21]. Genes closest to Sir2-dependent condensin peaks after subtraction of GFP are listed in Table S1, and are distributed throughout the genome. One of the strongest peaks overlapped with a Sir2-myc binding site on chromosome III between *KAR4* and *SPB1* that was not enriched for GFP (Fig 1A). The specificity of Sir2 enrichment at this peak, as opposed to the adjacent *SPB1* gene, was independently confirmed by quantitative ChIP using an α-Sir2 antibody (Fig 1B), with enrichment comparable to levels observed at the *HML-I* silencer (Fig 1A and B). Sir2-dependent condensin binding was also confirmed for Myc-tagged Smc4 and Brn1 subunits (Fig 1C). The ~2.5 kb intergenic region between *KAR4* and *SPB1* was previously defined as a cis-acting recombination enhancer (RE) that specifies donor preference of mating-type switching in *MAT*a cells [10, 13]. Quantitative ChIP assays revealed that Sir2 and Brn1-myc enrichment at the RE was also *MAT*a-specific (Fig 1D and E), which was notable because the ChIP-seq datasets in Fig 1A happened to be generated from *MAT*a strains. We next considered

whether condensin binding in the *MAT*a *sir2*Δ mutant was due to *HMLALPHA2* expression caused by defective *HML* silencing. To test this idea, we retested Brn1-myc ChIP at the RE in strains lacking *HML*, and found that deleting *SIR2* no longer affected condensin recruitment (Fig 1F). Similarly, a *MAT*a condensin mutant (*ycs4-1*) known to have an *HML* silencing defect [22] reduced Sir2 recruitment to the RE, but had no effect when *HML* was deleted (Fig 1G). Sir2 and condensin are therefore independently recruited to the RE specifically in *MAT*a cells.

Sir2 regulates a small gene (*RDT1*) within the RE

Donor preference activity ascribed to the RE was previously narrowed down to a *KAR4 (YCL055W)*-proximal 700 bp domain defined by an Mcm1/α2 binding site (Fig 2A, *DPS1*) [10, 11, 13]. The Sir2 and condensin ChIP-seq peaks we identified were located outside this region, between a second Mcm1/α2 binding site (*DPS2*) and a small gene of unknown function called *RDT1* [23] (Fig 1A and 2A). We noticed the location of *RDT1* coincided with the smallest of several putative non-coding RNAs (ncRNA) previously reported as being transcribed from the RE, but not annotated in SGD [24, Fig 2A]. Quantitative RT-PCR and analysis of publicly available RNA-seq data from BY4741 (*MAT*a) and BY4742 (*MAT*α) revealed that *RDT1* expression was indeed *MAT*a specific (Fig 2B and S1A).

We next asked whether Sir2 and/or condensin regulate histone acetylation and *RDT1* expression when recruited to the RE. Sir2 normally represses transcription at *HML*, *HMR*, and telomeres as a catalytic subunit of the SIR complex where it preferentially deacetylates H4K16 (reviewed in [5]). Accordingly, deleting *SIR2*, *SIR3*, or *SIR4* from *MAT*a cells increased H4K16 acetylation at the *RDT1* promoter (Fig 2C), consistent with the observed enrichment of Sir3-myc and Sir4-myc at this site (Fig S1B). Furthermore, re-introducing active *SIR2* into the *sir2*Δ

mutant restored H4K16 to the hypoacetylated state, whereas catalytically inactive *sir2-H364Y* did not (Fig 2D).

Deleting *SIR2* initially appeared to repress *RDT1* expression in *MAT*a cells (Fig 2E), but we hypothesized this was due to *HMLALPHA2* derepression and formation of the Mcm1/α2 repressor, which could locally repress *RDT1* through the adjacent Mcm1/α2 binding sites. Indeed, simultaneously deleting *SIR2* and *HML* resulted in very high *RDT1* expression (Fig 2E), which was increased even further when the paralogous *HST1* gene was also deleted (Fig S1C), indicating some redundancy. By eliminating *HML* we also observed elevated histone H3 acetylation in the absence of *SIR2* (Fig 2F), providing strong evidence that the SIR complex establishes a generally hypoacetylated chromatin environment at the *RDT1* promoter that requires effective silencing at *HML*. On the other hand, *RDT1* was not upregulated in an *hml*Δ *ycs4-1* condensin mutant (Fig 2G), suggesting that condensin has a different functional role at this locus.

We next attempted to block Sir2 and condensin recruitment to the *RDT1* promoter by precisely deleting a 100bp DNA sequence underlying the shared enrichment region (coordinates 30701-30800), while not disturbing the adjacent Mcm1/α2 site (Fig 3A). Sir2 and Brn1-myc binding to the RE as measured by ChIP was greatly diminished in this mutant (Fig 3B and 3C), despite unaltered Sir2, Brn1-myc, or Smc4-myc expression levels (Fig S2A-C). Furthermore, *RDT1* transcriptional expression was significantly increased by the 100bp deletion exclusively in *MAT*a cells (Fig 3D), consistent with the loss of Sir2-mediated repression.

Because Sir2 and condensin were not present at the *RDT1* promoter in *MAT*α cells, we reasoned that their binding should require a *MAT*a specific transcription factor. This made the 2nd Mcm1/α2 binding site (DPS2) upstream of the Sir2/condensin ChIP-seq peaks an ideal candidate

because it has not been ascribed a function other than redundancy with DPS1. Deleting *MCM1* is lethal, so alternatively, we deleted the 2nd Mcm1/α2 binding site (ChrIII coordinates 30595 to 30626, Fig S3A) and then retested for Sir2 and Brn1-myc enrichment. As shown in Fig S3B and S3C, respectively, Sir2 and Brn1-myc enrichment at both the Mcm1/α2 binding site (DPS2) and the *RDT1* promoter (defined as the Sir2/condensin peaks) was significantly reduced in the binding site mutant. These results suggest that Mcm1 may nucleate a complex that recruits the SIR and condensin complexes to the *RDT1* promoter in *MAT*a cells, and also provides a possible mechanism of blocking the recruitment in *MAT*α cells due to the interaction of Mcm1 with α2.

RDT1 encodes a translated mRNA

Ribosome Detected Transcript-1 (*RDT1*) was originally annotated as a newly evolved gene whose transcript was associated with ribosomes and predicted to have a small open reading frame of 28 amino acids [23]. Our work suggested that *RDT1* and the putative non-coding R2 transcript were the same (Fig 2A). To determine if *RDT1*/R2 codes for a small protein, the ORF was C-terminally fused with a 13x-Myc epitope in *MAT*a and *MAT*α cells. As shown in Fig 3E, a fusion protein was detectable in exponentially growing *MAT*a WT cells and also highly expressed in the 100bpΔ background, correlating with the increased RNA level observed for that mutant in Fig 3D.

Additional *MAT*a-specific RNAs are derived from the minimal 700bp RE domain (Fig 2A; R1L and R1S) [13, 25], so we next tested whether Sir2 controls their expression from a distance. As shown in Fig 3F, qRT-PCR using standard oligo(dT) primers for cDNA synthesis effectively measured *RDT1* expression at predicted levels for the various strains tested, but the R1 RNAs were not detectable. Many long non-coding RNAs (lncRNAs) are not polyadenylated

199 [26], so the cDNA synthesis was repeated using random hexamer primers. In *MAT*a WT cells
200 (ML1), R1L/S RNAs were now detected at levels comparable to *RDT1* (Fig 3G). Similar to
201 *RDT1*, R1L/S RNAs were repressed in the absence of *SIR2* due to the *HMLALPHA2*
202 pseudodiploid derepression phenotype. But unlike *RDT1*, the R1L/S RNA expression level was
203 not elevated in the 100bpΔ or *hml*Δ *sir2*Δ mutants, indicating these RNAs are not under direct
204 Sir2 control, but are strongly repressed in the absence of Sir2. We conclude that the R1L/S
205 RNAs are most likely non-polyadenylated lncRNAs, whereas *RDT1* is Sir2-repressed and
206 polyadenylated mRNA that can be translated into a small protein of unknown function.
207
208 **Sir2 and condensin are displaced from the *RDT1* promoter during mating-type switching**
209 We next asked if Sir2 played any role in regulating *RDT1* during mating-type switching. Sir2
210 was previously shown to associate with a HO-induced DSB at the *MAT* locus during mating-type
211 switching, presumably to effect repair through histone deacetylation [27]. Transient Sir2
212 recruitment to the DSB could potentially occur at expense of the *RDT1* promoter, thus resulting
213 in *RDT1* derepression. To test this idea, HO was induced at time 0 with galactose and then turned
214 off 2 hours later by glucose addition to allow for repair/switching to occur (Fig 4A and B). By
215 the 3 hr time point (1hr after glucose addition), ChIP analysis indicated Sir2 was maximally
216 enriched at the *MAT* locus (Fig 4C), corresponding to the time of peak mating-type switching
217 ([27] and Fig 4B). Interestingly. Sir2 was significantly depleted from the *RDT1* promoter within
218 1 hr after HO induction, and by 3 hr there was actually stronger enrichment of Sir2 at *MAT* than
219 *RDT1* (Fig 4C). Critically, this apparent Sir2 redistribution coincided with maximal induction of
220 *RDT1* mRNA and the Myc-tagged Rdt1protein (Fig 4D and 4E, 3 hr). Once switching was
221 completed by 4 hr (2hr after glucose addition), *RDT1* transcription was permanently inactivated

and Sir2 binding never returned because most cells were now *MAT*α. The Myc-tagged Rdt1 protein, however, remained elevated for the rest of the time course (Fig 4E), suggesting that it is relatively stable, at least when epitope tagged. A parallel ChIP time course experiment was performed with condensin (Brn1-myc), resulting in significant depletion from the *RDT1* promoter within 1 hr (Fig 4F), similar to the timing of Sir2 loss. However, rather than redistributing to the DSB, Brn1-myc enrichment was actually reduced at the break site, suggesting that condensin normally associates with *MAT*a in non-switching cells, but becomes displaced in response to the HO-induced DSB, perhaps to facilitate structural reorganization associated with switching.

The *RDT1* promoter region controls chromosome III architecture

The coupling of Sir2 and condensin distribution with *RDT1* transcriptional regulation during mating-type switching was reminiscent of classic locus control regions (LCR) that modulate long-range chromatin interactions. We therefore hypothesized that the *RDT1* promoter region may function as an LCR to modulate long-range chromatin interactions of chromosome III. To test this hypothesis, we performed Hi-C analysis with WT, *sir2*Δ and the 100bpΔ strains. Genomic contact differences between the mutants and WT were quantified using the HOMER Hi-C software suite [28], and the frequency of statistically significant differences for each chromosome calculated (Fig 5A). Chromosome III had the most significant differences in both mutants, so we focused on this chromosome and used HOMER to plot the observed/expected interaction frequency in 10kb bins for each strain as a heat map (Fig 5B). In a WT strain (ML1) there was strong interaction between the left and right ends of chromosome III, mostly centered around the *HML* (bin 2) and *HMR* (bin 29) loci. Interestingly, *HML* (bin 2) also appeared to

sample the entire right arm of chromosome III, with the interaction frequency increasing as a gradient from *CEN3* to a maximal observed interaction at *HMR*, thus also encompassing the *MAT*a locus at bin 20. This distinct interaction pattern was completely disrupted in the *sir2*Δ mutant, whereas some telomere-telomere contact was retained in the 100bpΔ mutant (Fig 5B), suggesting there was still limited interaction between the left and right ends of the chromosome. We confirmed the changes in *HML-HMR* interaction for these strains using a quantitative 3C-PCR assay to rule out sequencing artifacts, and also confirmed an earlier *sir2*Δ 3C result from the Dekker lab [29]. Importantly, despite the loss of *HML-HMR* interaction in the 100bpΔ mutant, heterochromatin at these domains was unaffected based on normal quantitative mating assays (Fig S4A), and unaltered Sir2 association with *HML* (Fig S4B).

We next analyzed the Hi-C data using an iterative correction method that reduces background to reveal interacting loci that potentially drive the overall chromosomal architecture, rather than passenger locus effects [30]. *HML* (bin 2) and *HMR* (bin 29) again formed the dominant interaction pair off the diagonal in WT, which was lost in the *sir2*Δ or 100bpΔ mutants (Fig 5D). Importantly, a prominent new interaction between *HMR* (bin 29) and *MAT*a (bin 20) appeared in both mutants (Fig 5D and E), as would be predicted if normal donor preference of *MAT*a cells was altered. We conclude that the *RDT1* promoter does function like an LCR in *MAT*a yeast cells, regulating localized transcription as well as long-range chromatin interactions relevant to mating-type switching (Fig 5E).

Sir2 and condensin regulate mating-type switching

Sir2/condensin binding was observed in the right half of the RE (Fig 1A), but this region was previously reported as being dispensable for donor preference activity [10]. Considering that

HMR was aberrantly associated with the *MAT*a locus in *sir2*Δ and 100bpΔ mutants (Fig 5), we proceeded to test whether these mutants had any alterations in donor preference. A reporter strain was used in which *HMR*a on the right arm of chromosome III was replaced with an *HMR*α allele containing a *Bam*HI site (*HMR*α-*B*) (Fig 6A). After inducing switching to *MAT*α following HO induction with galactose, the proportion of *HML*α or *HMR*α–B utilization for switching was determined by *Bam*HI digestion of a *MAT*α-specific PCR product (Fig 6B) [15]. As expected for normal donor preference, *HMR*α–B on the right arm was only utilized ~9% of the time in the WT strain, as compared to 91% for *HML*α (Fig 6C). Strikingly, donor preference was completely lost in the *sir2*Δ mutant, similar to a control strain with the RE deleted (Fig 6C and D), and consistent with the clear interaction between *HMR* and *MAT*a observed for the *sir2*Δ mutant in Fig 5D and E. This interaction was less prominent in the 100bpΔ mutant (Fig 5D), and the change in donor preference was also less severe (~25% *HMR*α-B), though still significantly different from WT (Fig 6C and D). Additionally, we measured the efficiency of switching to *MAT*α across a time course in the ML1 strain background used for ChIP and Hi-C analyses, and did not observe a significant difference between WT and the 100bpΔ mutant. However, switching to *MAT*α was severely impaired in the *sir2*Δ mutant (Fig 6E). We suspect the larger effect on switching efficiency and donor preference in *sir2*Δ cells is due to the derepression of *HMLALPHA2*, because α2 protein normally inactivates the RE in *MAT*α cells [13]. Silencing of *HML* is therefore critical for donor preference in the mating-type switching of *MAT*a cells by preventing expression of the repressive α2 transcription factor.

Since condensin is also recruited to the *RDT1* promoter region, we were next interested in whether condensin activity was important for mating-type switching. Each gene for the condensin subunits is essential, so instead of using deletions, in the ML1 strain background we

C-terminally tagged the Brn1 subunit with an auxin-inducible degron (AID) fused with a V5 epitope. This system allows for rapid depletion of tagged proteins upon addition of auxin to the growth media [31]. Indeed, Brn1-AID was effectively degraded within 15 min of adding auxin (Fig S5A). Importantly, even after 1 hr of auxin treatment, there were no changes in *RDT1* or *HMLALPHA2* gene expression indicated by qRT-PCR (Fig S5B and C), indicating that silencing of *HML* was unaffected, unlike the *ycs4-1* condensin mutant used in Fig 1G [22]. The efficiency of ML1 switching from *MAT*a to *MAT*α was then tested across a time course with or without auxin treatment (Fig 7A). As shown in Fig 7B and C, auxin treatment significantly slowed the pace of switching to *MAT*α, which also suggested there could be a modest effect on donor preference similar to that observed with the 100bpΔ strain. Indeed, Brn1-AID depletion produced a minor, yet significant, alteration in donor preference using the *HMR*α-B reporter strain (Fig 7D). Taken together, these results support a model whereby condensin recruited to the *RDT1* promoter in *MAT*a cells organizes chromosome III into a conformation that favors association of the *MAT*a locus with *HML* instead of *HMR*, thus partially contributing to donor preference regulation.

Discussion

SIR2 was identified almost 40 years ago as a recessive mutation unlinked from *HML* and *HMR* that caused their derepression [3, 4], and has been extensively studied ever since as encoding a heterochromatin factor that functions not only at the *HM* loci, but also telomeres and the rDNA locus (reviewed in [5]). In this study we describe a previously unidentified Sir2 binding site that overlaps with a major non-rDNA condensin binding site within the RE on chromosome III in *MAT*a cells. Here, Sir2 regulates a small gene of unknown function called *RDT1*, which is

transcriptionally activated during mating-type switching due to redistribution of repressive Sir2 from the *RDT1* promoter to the HO-induced DSB at *MAT*a. The *RDT1* RNA transcript is also polyadenylated and translated into a small protein, but we have not yet been able to assign a function to the gene or protein because deleting the 28 amino acid ORF had no measurable effect on mating-type switching when using the *GAL-HO* based assays tested thus far (data not shown). It remains possible that deleting *RDT1* would have a significant effect on switching in the context of native HO expression, which is expressed only in mother cells during late G1, whereas the *GAL1-HO* is overexpressed in all cells throughout the cell cycle. It is also possible that *RDT1* functions as a non-coding RNA that happens to be translated into a small non-functional peptide. Alternatively, transcription of *RDT1* could directly function in chromosome III conformation by altering local chromatin accessibility at the promoter. Such a model was proposed for regulation of donor preference by transcription of the R1S/R1L non-coding RNAs [13, 25]. Dissecting the function(s) of *RDT1* therefore remains an area of active investigation for the lab, and perhaps the key to fully understanding how its promoter functions as an LCR.

Functional complexity within the RE

While we do not yet know the molecular function of *RDT1* in mating-type regulation or other cellular processes, the promoter region of this gene clearly controls the structure of chromosome III. Three-dimensional chromatin structure has long been proposed to influence donor preference [32, 33]. However, deleting the minimal 700bp (left half) of the RE alters donor preference without a large change in chromosome III conformation. Furthermore, deleting the right half of the RE, which includes *RDT1*, changes chromosome III conformation without a dramatic change in donor preference [10, 13, 34]. Based on these findings it was proposed that

337 the RE is a bipartite regulatory element [34], with the left half primarily responsible for donor
338 preference activity and the right half for chromosome III structure. Our results support this view
339 and narrow down the structural regulatory domain of the RE to a small (100bp) region of the
340 *RDT1* promoter bound by the SIR and condensin complexes. Importantly, deleting this small
341 region not only altered chromosome III structure, but also had a significant effect on donor
342 preference, though not as strong as the *sir2*Δ mutation.

343 The coordination of *RDT1* expression with loss of Sir2/condensin binding at its promoter
344 during mating-type switching, together with the loss of *HML-HMR* interaction in the 100bpΔ
345 mutant, makes this site intriguingly similar to classic locus control regions (LCRs) in metazoans,
346 which are cis-acting domains that contain a mixture of enhancers, insulators, chromatin opening
347 elements, and tissue-specificity elements [35]. The minimal RE was previously described as an
348 LCR in the context of donor preference [10], and transcription of the R1S/R1L long non-coding
349 RNAs via activation by the 1st Mcm1/α2 binding site (DPS1) appears to be important for this
350 activity in *MAT*a cells [25]. We find that Sir2 indirectly supports donor preference from the left
351 half of the RE in *MAT*a cells by silencing *HMLALPHA2* expression, which prevents
352 transcriptional repression by an Mcm1/α2 heterodimer. Similarly, the loss of Sir2 also represses
353 *RDT1* expression and condensin recruitment in the right half of the RE due to *HMLALPHA2*
354 expression. However, Sir2 directly represses *RDT1* through localized histone deacetylation. How
355 the loss of *RDT1* regulation and condensin recruitment changes chromosome III structure in the
356 *sir2*Δ mutant remains unknown, but we propose that the *HMR-MAT*a interaction is a default
357 state, while the *HML-HMR* association has to be actively maintained by condensin and likely
358 additional factors co-localized to this element.

359 Interestingly, there also appears to be a function relationship between the RE and
360 silencing at the *HML* locus, such that deleting the left half of the RE specifically stabilizes *HML*
361 silencing in *MAT*a cells [36]. The mechanism involved remains unknown, but we hypothesize
362 that eliminating this part of the RE could potentially allow the SIR and condensin complexes
363 bound at the *RDT1* promoter encroach and somehow enhance the heterochromatic structure at
364 *HML*. Under this scenario, the left half of the RE could be insulating *HML* from the
365 chromosomal organizing activity that occurs at the *RDT1* promoter.
366
367 **Condensin function in mating-type switching**
368 The *RDT1* promoter was a major condensin binding site identified by ChIP-seq (Fig 1),
369 and given the strong Hi-C interaction between nearby *HML* and the *HMR* locus, we initially
370 hypothesized that condensin at the *RDT1* promoter would crosslink with another condensin site
371 bound on the right arm of chromosome III. ChIP-seq of Smc4-myc did not reveal any strong
372 peaks near *HMR*, but condensin was clearly enriched at *CEN3* (data not shown). Interestingly,
373 the *S. cerevisiae* condensin complex was recently shown to catalyze ATP-dependent
374 unidirectional loop extrusion using an *in vitro* single molecule assay [37]. The mechanism
375 involves direct binding of condensin to DNA, followed by one end of the bound DNA being
376 pulled inward as an extruded loop. Applying this model to the strong binding site at the *RDT1*
377 promoter, this region could act as an anchor bound by condensin, with DNA to the right being
378 rapidly extruded as a loop until pausing at *CEN3*. Extrusion would then continue at a slower rate
379 toward *HMR*, allowing *HML* the time to sample the entire right arm of chromosome III, until
380 clustering with *HMR*. HOMER analysis of the Hi-C data in Fig 5B provides evidence for such a
381 model because there is an ascending gradient of *HML* interaction frequency with sequences

382 extending from the centromere region (bin 2) toward *HMR*, suggesting that *HML* "samples" the
383 right arm of chromosome III. Once brought in contact, *HML* and *HMR* would then remain
384 associated due to their heterochromatic states and shared retention at the nuclear envelope [38] In
385 addition to preventing *HMR* association with *MAT*a, we hypothesize that the looped chromosome
386 III structure makes the chromosome licensed for mating-type switching in response to the HO-
387 induced DSB during G1.
388
389 **_MAT_a specific recruitment of Sir2 and condensin to the RE**
390 Condensin, and Sir2 each strongly associated with the *RDT1* promoter exclusively in *MAT*a
391 cells, though it is not clear if they bind at the same time, or are differentially bound throughout
392 the cell cycle. Since DPS2 was required for Sir2 and condensin recruitment, and derepression of
393 *HMLALPHA2* from *HML* also eliminated binding, we hypothesized and then demonstrated (Fig
394 S3) that Mcm1 was a key DNA binding factor involved. Mcm1 is a prototypical MADS box
395 combinatorial transcription factor that derives its regulatory specificity through interactions with
396 other factors, such as Ste12 in the case of *MAT*a haploid-specific gene activation, or α2 when
397 repressing the same target genes in *MAT*α cells [39]. This raises the question of whether Mcm1
398 directly recruits the SIR and condensin complexes, or perhaps additional factors that work with
399 Mcm1 are involved. At the *RDT1* promoter, specificity for Sir2/condensin recruitment could
400 originate from sequences underlying the condensin/Sir2 peaks. There are no traditional silencer-
401 like sequences for SIR recruitment within the deleted 100bp (coordinates 30702 to 30801), and
402 yeast condensin does not appear to have a consensus DNA binding sequence [40]. Closer
403 inspection of the *RDT1* promoter indicates an A/T rich region with consensus binding sites for
404 the transcription factors Fkh1/2 and Ash1, each of which regulates mating-type switching [11,

41, 42]. Fkh1 and Fkh2 also physically associate with Sir2 at the mitotic cyclin *CLB2* promoter during stress [43]. Ash1 is intriguing because it represses HO transcription in daughter cells [42, 44], raising the possibility of *RDT1* repression in daughter cells. Mcm1 activity in *MAT*a cells could also indirectly establish a chromatin environment that is competent for Sir2/condensin recruitment, rather than direct recruitment through protein-protein interactions. In *MAT*a cells, Mcm1 appears to prevent the strong nucleosome positioning across the RE that occurs in *MAT*α cells [25], and indicative of an actively remodeled chromatin environment. Perhaps condensin is attracted to such regions, which is consistent with the association of condensin with promoters of active genes in mitotic cells, where enrichment was greatest at unwound regions of DNA [45]. Furthermore, nucleosome eviction by transcriptional coactivators was found to assist condensin loading in yeast [46], though the mechanism of loading remains poorly understood. Recruitment of condensin to the *RDT1* promoter LCR therefore provides an outstanding opportunity for dissecting mechanisms of condensin loading and function.

Methods

Yeast strains, plasmids, and media

Yeast strains were grown at 30°C in YPD or synthetic complete (SC) medium where indicated. The *SIR2*, or *HST1* open reading frames (ORFs) were deleted with *kanMX4* using one-step PCR-mediated gene replacement. *HML* was deleted and replaced with *LEU2*. A 100bp deletion within the *RDT1* promoter (chrIII coordinates 30701-30800) or DPS2 deletion (chrIII coordinates 30557-30626) was generated using the *delitto perfetto* method [47]. Endogenous *SIR2*, *BRN1*, or *SMC4* genes were C-terminally tagged with the 13xMyc epitope (13-EQKLISEEDL). Deletion and tagged genes combinations were generated through genetic crosses and tetrad dissection,

including Brn1 tagged with a V5-AID tag (template plasmids kindly provided by Vincent Guacci). All genetic manipulations were confirmed by PCR, and expression of tagged proteins confirmed by western blotting. The pGAL-HO-URA3 expression plasmid was kindly provided by Jessica Tyler [27]. Strain genotypes are provided in Supplemental Table S2 and oligonucleotides listed in Table S3.

ChIP-Seq analysis

Sir2 ChIP-seq was previously described [19]. For other ChIP-seq datasets, log-phase YPD cultures were cross-linked with 1% formaldehyde for 20 min, pelleted, washed with Tris-buffered saline (TBS), and then lysed in 600 µl FA140 lysis buffer with glass beads using a mini-beadbeater (BioSpec Products). Lysates were removed from the beads and sonicated for 60 cycles (30s "on" and 30s "off" per cycle) in a Diagenode Bioruptor. Sonicated lysates were pelleted for 5 min at 14000 rpm in a microcentrifuge and the entire supernatant was transferred to a new microfuge tube and incubated overnight at 4°C with 5 µg of anti-Myc antibody (9E10) and 20 µl of protein G magnetic beads (Millipore). Following IP, the beads were washed once with FA140 buffer, twice with FA500 buffer, and twice with LiCl wash buffer. DNA was eluted from the beads in 1% SDS/TE buffer and cross-links were reversed overnight at 65°C. The chromatin was then purified using a Qiagen PCR purification kit. Libraries were constructed using the Illumina Trueseq ChIP Sample Prep kit and TrueSeq standard protocol with 10ng of initial ChIP or Input DNA. Libraries that passed QC on a Bioanalyzer High Sensitivity DNA Chip (Agilent Technologies) were sequenced on an Illumina Miseq (UVA DNA Sciences Core).

ChIP-seq computational analysis

Biological duplicate fastq files were concatenated together and reads mapped to the sacCer3 genome using Bowtie with the following options: ---best, --stratum, --nomaqround, and --m10 [48]. The resulting bam files were then converted into bigwig files using BEDTools [49]. As part of the pipeline, chromosome names were changed from the sacCer3 NCBI values to values readable by genomics viewers e.g. "ref|NC_001133|" to "chrI". The raw and processed datasets used in this study have been deposited in NCBI's GEO and are accessible through the GEO series accession number GSE92717. Downstream GO analysis was performed as follows. MACS2 was used to call peaks with the following options: --broad, --keep-dup, -tz 150, and -m 3, 1000 [50]. GFP peaks in the WT or *sir2*Δ backgrounds were subtracted from the WT *SMC4-13xMyc* and *sir2*Δ *SMC4-13xMyc* peaks, respectively, using BEDTools "intersect" with the –v option. The resulting normalized peaks were annotated using BEDTools "closest" with the -t all option specified, and in combination with a yeast gene list produced from USCS genome tables. The annotated peaks were then analyzed for GO terms using YeastMine (yeastmine.yeastgenome.org).

Hi-C analysis

Log-phase cultures were cross-linked with 3% formaldehyde for 20 min and quenched with a 2x volume of 2.5M Glycine. Cell pellets were washed with dH_2O and stored at -80°C. Thawed cells were resuspended in 5 ml of 1X NEB2 restriction enzyme buffer (New England Biolabs) and poured into a pre-chilled mortar containing liquid N_2. Nitrogen grinding was performed twice as previously described [51], and the lysates were then diluted to an OD_{600} of 12 in 1x NEB2 buffer. 500 µl of cell lysate was used for each Hi-C library as follows. Lysates were solubilized by the addition of 50 µl 1% SDS and incubation at 65°C for 10 min. 55 µl of 10% TritonX-100 was

added to quench the SDS, followed by 10 µl of 10X NEB2 buffer and 15 µl of *Hin*dIII (New England Biolabs, 20 U/µl) to digest at 37°C for 2 hr. An additional 10 µl of *Hin*dIII was added for digestion overnight. The remainder of the protocol was based on previously published work with minor exceptions [52]. In short, digested chromatin ends were filled-in with Klenow fragment (New England Biolabs) and biotinylated dCTP at 37°C for 1 hr, then heat inactivated at 70°C for 10 min. Ligation reactions with T4 DNA ligase were performed at 16°C for a minimum of 6 hr using the entire Hi-C sample diluted into a total volume of 4 ml. Proteinase K was added and cross-links were reversed overnight at 70°C. The ligated chromatin was phenol:chloroform extracted, ethanol precipitated, then resuspended in 500µl dH_2O and treated with RNAse A for 45 min. Following treatment with T4 DNA polymerase to remove biotinylated DNA ends that were unligated, the samples were concentrated with a Clean and Concentrator spin column (Zymogen, D4013) and sheared to approximately 300bp with a Diagenode Bioruptor. Biotinylated fragments were captured with 30 µl pre-washed Streptavidin Dynabeads (Invitrogen), then used for library preparation. Hi-C sequencing libraries were prepared with reagents from an Illumina Nextera Mate Pair Kit (FC-132-1001) using the standard Illumina protocol of End Repair, A-tailing, Adapter Ligation, and 12 cycles of PCR. PCR products were size selected and purified with AMPure XP beads before sequencing with an Illumina Miseq or Hiseq. Raw and mapped reads deposited at GEO (GSE92717).

Hi-C computational analysis

Iteratively corrected heatmaps were produced using python scripts from the Mirny lab hiclib library, http://mirnylab.bitbucket.org/hiclib/index.html. Briefly, reads were mapped using the iterative mapping program, which uses Bowtie2 to map reads and iteratively trims unmapped

497 reads to increase the total number of mapped reads. Mapped reads were then parsed into an hdf5
498 python data dictionary for storage and further analysis. Mapped reads of the same strains were
499 concatenated using the hiclib library's “Merge" function. Both individual and concatenated
500 mapped reads have been deposited in GEO. Mapped reads were then run through the fragment
501 filtering program using the default parameters as follows: filterRsiteStart(offset=5),
502 filterDuplicates, filterLarge, filterExtreme (cutH=0.005, cutL=0). Raw heat maps were further
503 filtered to remove diagonal reads and iteratively corrected using the 03 heat map processing
504 program. Finally, the iteratively corrected heatmaps were normalized for read count differences
505 by dividing the sum of each row by the sum of the max row for a given plot, which drives all
506 values towards 1 to make individual heatmaps comparable.
507 Observed/Expected heatmaps were created using HOMER Hi-C analysis software on the
508 BAM file outputs from the iterativemapping program of the hiclib library python package [28].
509 Tag directories were created using all experimental replicates of a given biological sample and
510 the tbp -1 and illuminaPE options. Homer was also used to score differential chromosome
511 interactions between the WT and mutant Hi-C heatmaps. The resulting list of differential
512 interactions was uploaded into R where the given p-value was adjusted to a qvalue with p.adjust.
513 An FDR cutoff of 0.05 was used to create a histogram of significantly different chromosome
514 interactions in the mutants compared to WT. The histogram was further normalized by dividing
515 the total number of significant differential interactions for a chromosome by total number of
516 interactions called in the WT sample for that chromosome to account for size differences in the
517 chromosomes. Thus, frequency represents the number of interactions that changed out of all
518 possible interactions that could have changed.
519

520 **RNA-seq data analysis**

521 RNA-Seq data was acquired from GEO accessions GSE73274 [53] and GSE58319 [54] for the
522 BY4742 (*MAT*α) and BY4741 (*MAT*a) backgrounds, respectively. Reads were then mapped to
523 the sacCer3 genome using Bowtie2 with no further processing of the resulting BAM files
524 visualized in this paper.

525

526 **3C assays**

527 Chromosome Conformation Capture (3C) was performed in a similar manner to Hi-C with a few
528 exceptions due to assay-specific quantification via quantitative real-time PCR rather than
529 sequencing. Most notably, digested DNA ends were not filled in with dCTP-biotin before
530 ligation and an un-crosslinked control library was created for each 3C library. Furthermore, all
531 PCR reactions were normalized for starting DNA concentration using a *PDC1* intergenic region
532 that is not recognized by *Hin*dIII, in addition to PCR of the un-crosslinked control for all tested
533 looping interaction primer pairs.

534

535 **Quantitative reverse transcriptase (RT) PCR assay**

536 Total RNA (1 μg) was used for cDNA synthesis with oligo(dT) and Superscript II reverse
537 transcriptase as previously described [55].

538

539 **Western blot**

540 Proteins were blotted using standard TCA extraction followed by SDS-PAGE as previously
541 described [19]. Myc-tagged proteins were incubated with an anti-Myc primary antibody 9E10
542 (Millipore) at a 1:2000 dilution while tubulin was incubated with anti-Tubulin antibody B-5-1-2

(Sigma-Aldrich) at a 1:1500 dilution. The V5-AID tagged Brn1 was detected with anti-V5 antibody (Invitrogen, R96025) at a 1:4000 dilution. Primary antibodies were detected with an anti-mouse secondary antibody conjugated to HRP (Promega) at 1:5000 dilution in 5% fat-free milk. Bands were then visualized with HyGlo (Denville Scientific) capture on autoradiography film (Denville Scientific).

Mating-type switching assays

For tracking the efficiency of switching, strains were transformed with pGAL-HO-*URA3*, pre-cultured in SC-ura + raffinose (2%) medium overnight, re-inoculated into the same medium (OD_{600}=0.05) and then grown into log phase. Galactose (2%) was added to induce HO expression for 45 min. Glucose (2%) was then added and aliquots of the cultures were harvested at indicated time points. Genomic DNA was isolated and 10 ng used for PCR amplification. *MAT*α was detected using primers JS301 and JS302. The *SCR1* gene on chromosome V was used as a loading control (primers JS2665 and JS2666). PCR products were separated on a 1% agarose gel stained with ethidium bromide and then quantified using ImageJ. Donor preference with strains containing *HMR*α-B was performed as previously described [15]. Briefly, MATa was amplified with primers Yalpha105F and MATdist-4R from genomic DNA 90 after switching was completed (90 min), and then digested with BamHI. Ethidium stained bands were quantified using ImageJ. For the conditional V5-AID degron strains, degradation of V5-AID-fused Brn1 protein was induced by addition of 0.5 mM indole-3-acetic acid (Auxin, Sigma # 13750).

Author contributions

Conceptualization; M.L., R.D.F., and J.S.S.; Methodology, M.L, R.D.F., M.D., and J.S.S.; Software, R.D.F. and S.B.; Strain Creation and Validation, M.L., R.D.F., and M.D., Plasmid Creation and Validation, M.L., and R.D.F.; Formal Analysis, M.L., R.D.F., and S.B.; Data Curation, R.D.F.; Writing-Original Draft, M.L., R.D.F. and J.S.S.; Writing Review & Editing, M.L., R.D.F., M.D., and J.S.S; Supervision, J.S.S. and S.B.; Project Administration, J.S.S.; Funding Acquisition, J.S.S.

Acknowledgments

We thank Job Dekker, Jon Belton, Maitreya Dunham, Ivan Liachko, Maxim Imakev, and Anton Goloborodko for advice on Hi-C protocols and analysis methods. We also thank James Haber, Andrew Murray, Jasper Rine, Jessica Tyler, Alan Hinnebusch, Marc Gartenberg, Dan Gottschling, and Vincent Guacci for kindly providing yeast strains, plasmids, or antibodies. We thank David Auble and Patrick Grant for reading the manuscript and providing suggestions prior to submission. We declare no conflicts of interest.

References

1. Haber JE. Mating-type genes and *MAT* switching in *Saccharomyces cerevisiae*. Genetics. 2012;191(1):33-64. PMID: 22555442.

2. Haber JE, George JP. A mutation that permits the expression of normally silent copies of mating-type information in *Saccharomyces cerevisiae*. Genetics. 1979;93(1):13-35. PMID: 16118901.

3. Klar AJ, Fogel S, Macleod K. *MAR1*-A regulator of the *HM*a and *HM*α loci in *Saccharomyces cerevisiae*. Genetics. 1979;93(1):37-50. PMID: 17248968.

4. Rine J. Regulation and Transposition of Cryptic Mating Type Genes in *Saccharomyces cerevisiae*. Eugene, OR: University of Oregon; 1979.

5. Gartenberg MR, Smith JS. The nuts and bolts of transcriptionally silent chromatin in *Saccharomyces cerevisiae*. Genetics. 2016;203(4):1563-99. PMID: 27516616.

6. Strathern JN, Klar AJ, Hicks JB, Abraham JA, Ivy JM, Nasmyth KA, et al. Homothallic switching of yeast mating type cassettes is initiated by a double-stranded cut in the *MAT* locus. Cell. 1982;31(1):183-92. PMID: 6297747.

7. Haber JE, Rogers DT, McCusker JH. Homothallic conversions of yeast mating-type genes occur by intrachromosomal recombination. Cell. 1980;22(1 Pt 1):277-89. PMID: 6253081.

8. Nasmyth K. The determination of mother cell-specific mating type switching in yeast by a specific regulator of HO transcription. EMBO J. 1987;6(1):243-8. PMID: 15981333.

9. Klar AJ, Hicks JB, Strathern JN. Directionality of yeast mating-type interconversion. Cell. 1982;28(3):551-61. PMID: 7042099.

10. Wu X, Haber JE. A 700 bp cis-acting region controls mating-type dependent recombination along the entire left arm of yeast chromosome III. Cell. 1996;87(2):277-85. PMID: 8861911.

11. Sun K, Coic E, Zhou Z, Durrens P, Haber JE. *Saccharomyces* forkhead protein Fkh1 regulates donor preference during mating-type switching through the recombination enhancer. Genes Dev. 2002;16(16):2085-96. PMID: 12183363.

12. Wu C, Weiss K, Yang C, Harris MA, Tye BK, Newlon CS, et al. Mcm1 regulates donor preference controlled by the recombination enhancer in *Saccharomyces* mating-type switching. Genes Dev. 1998;12(11):1726-37. PMID: 9620858.

611 13. Szeto L, Fafalios MK, Zhong H, Vershon AK, Broach JR. α2p controls donor preference
612 during mating type interconversion in yeast by inactivating a recombinational enhancer of
613 chromosome III. Genes Dev. 1997;11(15):1899-911. PMID: 9271114.
614 14. Dummer AM, Su Z, Cherney R, Choi K, Denu J, Zhao X, et al. Binding of the Fkh1
615 forkhead associated domain to a phosphopeptide within the Mph1 DNA helicase regulates
616 mating-type switching in budding yeast. PLoS Genet. 2016;12(6):e1006094. PMID: 27257873.
617 15. Li J, Coic E, Lee K, Lee CS, Kim JA, Wu Q, et al. Regulation of budding yeast mating-
618 type switching donor preference by the FHA domain of Fkh1. PLoS Genet. 2012;8(4):e1002630.
619 PMID: 22496671.
620 16. Jensen R, Sprague GF, Jr., Herskowitz I. Regulation of yeast mating-type
621 interconversion: feedback control of *HO* gene expression by the mating-type locus. Proc Natl
622 Acad Sci U S A. 1983;80(10):3035-9. PMID: 6344075.
623 17. Klar AJ, Hicks JB, Strathern JN. Irregular transpositions of mating-type genes in yeast.
624 Cold Spring Harb Symp Quant Biol. 1981;45 Pt 2:983-90. PMID: 6266771.
625 18. Nasmyth KA. The regulation of yeast mating-type chromatin structure by SIR: an action
626 at a distance affecting both transcription and transposition. Cell. 1982;30(2):567-78. PMID:
627 6215985.
628 19. Li M, Valsakumar V, Poorey K, Bekiranov S, Smith JS. Genome-wide analysis of
629 functional sirtuin chromatin targets in yeast. Genome Biol. 2013;14(5):R48. PMID: 23710766.
630 20. D'Ambrosio C, Schmidt CK, Katou Y, Kelly G, Itoh T, Shirahige K, et al. Identification
631 of cis-acting sites for condensin loading onto budding yeast chromosomes. Genes Dev.
632 2008;22(16):2215-27. PMID: 18708580.

633 21. Teytelman L, Thurtle DM, Rine J, van Oudenaarden A. Highly expressed loci are
634 vulnerable to misleading ChIP localization of multiple unrelated proteins. Proc Natl Acad Sci U
635 S A. 2013;110(46):18602-7. PMID: 24173036.
636 22. Bhalla N, Biggins S, Murray AW. Mutation of *YCS4*, a budding yeast condensin subunit,
637 affects mitotic and nonmitotic chromosome behavior. Mol Biol Cell. 2002;13(2):632-45. PMID:
638 11854418.
639 23. Wilson BA, Masel J. Putatively noncoding transcripts show extensive association with
640 ribosomes. Genome Biol Evol. 2011;3:1245-52. PMID: 21948395.
641 24. Szeto L, Broach JR. Role of α2 protein in donor locus selection during mating type
642 interconversion. Mol Cell Biol. 1997;17(2):751-9. PMID: 9001229.
643 25. Ercan S, Reese JC, Workman JL, Simpson RT. Yeast recombination enhancer is
644 stimulated by transcription activation. Mol Cell Biol. 2005;25(18):7976-87. PMID: 16135790.
645 26. Yang L, Duff MO, Graveley BR, Carmichael GG, Chen LL. Genomewide
646 characterization of non-polyadenylated RNAs. Genome Biol. 2011;12(2):R16. PMID: 21324177.
647 27. Tamburini BA, Tyler JK. Localized histone acetylation and deacetylation triggered by the
648 homologous recombination pathway of double-strand DNA repair. Mol Cell Biol.
649 2005;25(12):4903-13. PMID: 15923609.
650 28. Heinz S, Benner C, Spann N, Bertolino E, Lin YC, Laslo P, et al. Simple combinations of
651 lineage-determining transcription factors prime cis-regulatory elements required for macrophage
652 and B cell identities. Mol Cell. 2010;38(4):576-89. PMID: 20513432.
653 29. Miele A, Bystricky K, Dekker J. Yeast silent mating type loci form heterochromatic
654 clusters through silencer protein-dependent long-range interactions. PLoS Genet.
655 2009;5(5):e1000478. PMID: 19424429.

656 30. Imakaev M, Fudenberg G, McCord RP, Naumova N, Goloborodko A, Lajoie BR, et al.
657 Iterative correction of Hi-C data reveals hallmarks of chromosome organization. Nat Methods.
658 2012;9(10):999-1003. PMID: 22941365.
659 31. Nishimura K, Fukagawa T, Takisawa H, Kakimoto T, Kanemaki M. An auxin-based
660 degron system for the rapid depletion of proteins in nonplant cells. Nat Methods.
661 2009;6(12):917-22. PMID: 19915560.
662 32. Coic E, Richard GF, Haber JE. *Saccharomyces cerevisiae* donor preference during
663 mating-type switching is dependent on chromosome architecture and organization. Genetics.
664 2006;173(3):1197-206. PMID: 16624909.
665 33. Wu X, Haber JE. *MAT*a donor preference in yeast mating-type switching: activation of a
666 large chromosomal region for recombination. Genes Dev. 1995;9(15):1922-32. PMID: 7649475.
667 34. Belton JM, Lajoie BR, Audibert S, Cantaloube S, Lassadi I, Goiffon I, et al. The
668 Conformation of yeast chromosome III is mating type dependent and controlled by the
669 recombination enhancer. Cell Rep. 2015;13(9):1855-67. PMID: 26655901.
670 35. Li Q, Peterson KR, Fang X, Stamatoyannopoulos G. Locus control regions. Blood.
671 2002;100(9):3077-86. PMID: 12384402.
672 36. Dodson AE, Rine J. Donor preference meets heterochromatin: Moonlighting activities of
673 a recombinational enhancer in *Saccharomyces cerevisiae*. Genetics. 2016;204(1):177-90. PMID:
674 27655944.
675 37. Ganji M, Shaltiel IA, Bisht S, Kim E, Kalichava A, Haering CH, et al. Real-time imaging
676 of DNA loop extrusion by condensin. Science. 2018;360(6384):102-5. PMID: 29472443.

677 38. Bystricky K, Van Attikum H, Montiel MD, Dion V, Gehlen L, Gasser SM. Regulation of
678 nuclear positioning and dynamics of the silent mating type loci by the yeast Ku70/Ku80
679 complex. Mol Cell Biol. 2009;29(3):835-48. PMID: 19047366.
680 39. Messenguy F, Dubois E. Role of MADS box proteins and their cofactors in combinatorial
681 control of gene expression and cell development. Gene. 2003;316:1-21. PMID: 14563547.
682 40. Wang BD, Eyre D, Basrai M, Lichten M, Strunnikov A. Condensin binding at distinct
683 and specific chromosomal sites in the *Saccharomyces cerevisiae* genome. Mol Cell Biol.
684 2005;25(16):7216-25. PMID: 16055730.
685 41. Bobola N, Jansen RP, Shin TH, Nasmyth K. Asymmetric accumulation of Ash1p in
686 postanaphase nuclei depends on a myosin and restricts yeast mating-type switching to mother
687 cells. Cell. 1996;84(5):699-709. PMID: 8625408.
688 42. Sil A, Herskowitz I. Identification of asymmetrically localized determinant, Ash1p,
689 required for lineage-specific transcription of the yeast *HO* gene. Cell. 1996;84(5):711-22. PMID:
690 8625409.
691 43. Linke C, Klipp E, Lehrach H, Barberis M, Krobitsch S. Fkh1 and Fkh2 associate with
692 Sir2 to control *CLB2* transcription under normal and oxidative stress conditions. Front Physiol.
693 2013;4:173. PMID: 23874301.
694 44. Long RM, Singer RH, Meng X, Gonzalez I, Nasmyth K, Jansen RP. Mating type
695 switching in yeast controlled by asymmetric localization of *ASH1* mRNA. Science.
696 1997;277(5324):383-7. PMID: 9219698.
697 45. Sutani T, Sakata T, Nakato R, Masuda K, Ishibashi M, Yamashita D, et al. Condensin
698 targets and reduces unwound DNA structures associated with transcription in mitotic
699 chromosome condensation. Nat Commun. 2015;6:7815. PMID: 26204128.

700 46. Toselli-Mollereau E, Robellet X, Fauque L, Lemaire S, Schiklenk C, Klein C, et al.
701 Nucleosome eviction in mitosis assists condensin loading and chromosome condensation.
702 EMBO J. 2016;35(14):1565-81. PMID: 27266525.
703 47. Storici F, Lewis LK, Resnick MA. *In vivo* site-directed mutagenesis using
704 oligonucleotides. Nat Biotechnol. 2001;19(8):773-6. PMID: 11479573.
705 48. Langmead B, Trapnell C, Pop M, Salzberg SL. Ultrafast and memory-efficient alignment
706 of short DNA sequences to the human genome. Genome Biol. 2009;10(3):R25. PMID:
707 19261174.
708 49. Quinlan AR, Hall IM. BEDTools: a flexible suite of utilities for comparing genomic
709 features. Bioinformatics. 2010;26(6):841-2. PMID: 20110278.
710 50. Liu T. Use model-based analysis of ChIP-Seq (MACS) to analyze short reads generated
711 by sequencing protein-DNA interactions in embryonic stem cells. Methods Mol Biol.
712 2014;1150:81-95. PMID: 24743991.
713 51. Belton JM, Dekker J. Measuring chromatin structure in budding yeast. Cold Spring Harb
714 Protoc. 2015;2015(7):614-8. PMID: 26134912.
715 52. Burton JN, Liachko I, Dunham MJ, Shendure J. Species-level deconvolution of
716 metagenome assemblies with Hi-C-based contact probability maps. G3 (Bethesda).
717 2014;4(7):1339-46. PMID: 24855317.
718 53. Porter DF, Koh YY, VanVeller B, Raines RT, Wickens M. Target selection by natural
719 and redesigned PUF proteins. Proc Natl Acad Sci U S A. 2015;112(52):15868-73. PMID:
720 26668354.

721 54. Swamy KB, Lin CH, Yen MR, Wang CY, Wang D. Examining the condition-specific
722 antisense transcription in *S. cerevisiae* and *S. paradoxus*. BMC Genomics. 2014;15:521. PMID:
723 24965678.
724 55. Li M, Petteys BJ, McClure JM, Valsakumar V, Bekiranov S, Frank EL, et al. Thiamine
725 biosynthesis in *Saccharomyces cerevisiae* is regulated by the NAD^+-dependent histone
726 deacetylase Hst1. Mol Cell Biol. 2010;30(13):3329-41. PMID: 20439498.

727

728 Figure captions

729 **Fig 1. *MAT*a-specific binding of Sir2 and condensin to the recombination enhancer (RE).**
730 **(A)** Chip-seq of Smc4-myc, Sir2-myc, and nuclear localized GFP in WT and *sir2*Δ backgrounds.
731 The left arm of chromosome III is depicted from *HML* to *SPB1*. RE indicates the recombination
732 enhancer region. Inset: The minimal 700bp RE element required for donor preference is
733 indicated, as are the two Mcm1/α2 binding sites (DPS1 and DPS2) and *RDT1*. **(B)** Sir2 ChIP at
734 the RE, *HML-I* silencer, and *SPB1*. **(C)** α-Myc ChIP of Brn1-myc and Smc4-myc at the RE. **(D)**
735 ChIP showing *MAT*a-specific binding of Sir2 to the RE. **(E)** ChIP showing *MAT*a-specific
736 binding of Brn1-myc to the RE. **(F)** Brn1-Myc ChIP at RE is not Sir2 dependent. **(G)** Native Sir2
737 ChIP at RE is not condensin dependent. ChIP signal relative to input is plotted as the mean of
738 three replicates. Error bars = standard deviation. (**p<0.005).

739

740 **Fig 2. *RDT1* is a novel Sir2 regulated gene (A)** Schematic of RE locus depicting
741 Sir2/Condensin peak location relative to previously reported R1L/S and R2 RNA (*RDT1*). **(B)**
742 *RDT1* mRNA expression is *MAT*a specific. **(C)** H4K16ac ChIP at RE in SIR complex null
743 strains. **(D)** H4K16ac deacetylation is dependent on Sir2 catalytic activity. A *sir2*Δ strain was

744 transformed with the indicated plasmids and ChIP assays performed. **(E)** Differential *RDT1*
745 transcriptional regulation by *SIR2* is dependent on *HML* status. **(F)** Effect of *sir2*Δ on
746 H3K9/K14ac ChIP at the *RDT1* promoter in *HML* and *hml*Δ backgrounds. **(G)** Effects of the
747 temperature sensitive *ycs4-1* mutation on *RDT1* expression in *HML* and *hml*Δ backgrounds.
748 (*p<0.05; **p<0.005).
749
750 **Fig 3. Identification of a 100bp sequence that recruits Sir2/condensin and represses RDT1**
751 **expression. (A)** Schematic indicating a 100bp deletion that covers the condensin (red) and Sir2
752 (blue) peaks. (B) ChIP of Sir2 in the 100bpΔ mutant (ML275). **(C)** ChIP of Brn1-Myc in the
753 100bpΔ mutant. **(D)** *RDT1* transcription in *MAT*a cells is derepressed in the 100bpΔ mutant. **(E)**
754 Western blot of Rdt1-13xMyc in WT *MAT*α and *MAT*a cells, as well as the *MAT*a 100bpΔ
755 mutant. **(F)** *RDT1* and R1 expression when using oligo dT priming for the reverse transcription
756 step. **(G)** *RDT1* and R1 expression when using random hexamer priming for reverse
757 transcription. (**p<0.005).
758
759 **Fig 4. Dynamics of Sir2 and condensin binding at the *RDT1* promoter and *MAT*a locus**
760 **during mating-type switching. (A, B)** Mating-type switching time course where HO was
761 induced by galactose at time 0, then glucose added at 2 hr to stop HO expression and allow for
762 break repair. Switching is maximal at 3 hr [27]. **(C)** ChIP of Sir2 at the *RDT1* promoter and the
763 HO-induced DSB (*MAT*-HO). **(D)** qRT-PCR of *RDT1* expression across the mating-type
764 switching time course. **(E)** Rdt1-13xMyc protein expression across the same time course. **(F)**
765 ChIP of Brn1-myc at the *RDT1* promoter and MAT-HO break site across the same time course.
766 (*p<0.05, **p<0.005 compared to time 0).

Fig 5. The Sir2/condensin binding site controls chromosome III architecture.

(A) Frequency of significant Hi-C interaction changes identified using HOMER for each chromosome in the *sir2*Δ (ML25) and 100bpΔ (ML275) strains compared to WT (ML1). **(B)** HOMER-generated observed/expected Hi-C interaction frequency heat maps (10kb bins) for chromosome III. **(C)** qPCR detection of *HML-HMR* interaction using 3C analysis. (*$p < 0.05$, **<0.005). **(D)** Iteratively corrected and read-normalized Hi-C heat maps revealing an interaction between *HMR* (bin 29) and *MAT*a (bin 20) in the *sir2*Δ and 100bpΔ mutants. **(E)** Summary of large-scale changes in chromosome III architecture. Δ indicates the 100bp deletion.

Fig 6. Loss of Sir2 and the Sir2/condensin binding site alters mating-type switching. (A) Schematic of a donor preference assay in which utilization of an artificial *HMR*α-B cassette as the donor for switching introduces a unique *Bam*HI site to the *MAT* locus. **(B)** Locations of primers flanking the *Bam*HI site used for PCR detection of *MAT*α. **(C)** Representative ethidium bromide stained agarose gel of *Bam*HI-digested *MAT*α PCR products after mating-type switching in WT (XW652), *re*Δ (XW676), *sir2*Δ (ML557), and 100bpΔ (SY742) strains. The *MAT*α-B product is digested into 2 smaller bands. **(D)** Quantifying the percentage of *MAT*α PCR product digested by *Bam*HI, from three biological replicates. ImageJ was used for the quantitation. (**$p < 0.005$). **(E)** Time course of switching from *MAT*a to *MAT*α in WT (ML447), 100bpΔ (ML460), and *sir2*Δ (ML458) strains after HO was induced for 45 min and then shut down with glucose. Aliquots were harvested at 30 min intervals. *SCR1* is a control for input genomic DNA. **(F)** ImageJ quantification of *MAT*α PCR relative to *SCR1* for each time point.

790 **Fig 7. Effects of condensin depletion on mating-type switching. (A)** Schematic of the time
791 course used to deplete Brn1-AID prior to the induction of mating-type switching in the ML1
792 strain background. Auxin was added 30 min prior to the induction of HO expression by
793 galactose. **(B)** EtBr stained agarose gel of *MAT*α PCR products amplified from each time point
794 during mating-type switching. *SCR1* PCR was used as a control for input DNA. **(C)**
795 Quantification of the *MAT*α/*SCR1* PCR product ratio across the time course from 3 biological
796 replicates. **(D)** Effect of Brn1-AID depletion on mating-type switching donor preference. A
797 representative biological replicate is shown, along with quantitation of switching using the
798 *HMR*α-B cassette.
799

800 ## Supporting Figure and Table Captions

801 **Fig S1. *MAT*a-specific transcription of *RDT1* is repressed by Sir2 and Hst1. (A)** IGV
802 screenshot of compiled raw RNA-seq read data from BY4741 (*MAT*a) and BY4742 (*MAT*α)
803 strains. The top two blue peaks represent Smc4-myc and Sir2-myc ChIP-seq reads. **(B)**
804 Quantitative ChIP assay showing additional SIR complex subunit enrichment at the *RDT1*
805 promoter. **(C)** RT-qPCR showing effects of deleting *SIR2* and/or *HST1* on *RDT1* expression
806 when HML is present or deleted (*p<0.05, **p<.005).
807

808 **Fig S2. Deletion of Sir2 or the *RDT1* promoter Sir2/condensin binding site does not affect**
809 **protein levels of Sir2 or Myc-tagged condensin subunits. (A)** Western blot showing steady
810 state Sir2 protein levels in WT (ML1), *sir2*Δ (ML25), and 100bpΔ (ML275) strains. **(B)** Western
811 blot with anti-Myc detection of Brn1-13xMyc or Sir2 in WT (ML149), *sir2*Δ (ML161), and

100bpΔ (ML322) strains. **(C)** Western blot with anti-Myc detection of Smc4-13xMyc or Sir2 in WT (ML152), *sir2*Δ (ML160), and 100bpΔ version.

Fig S3. The *RDT1*-proximal Mcm1/a2 binding site (DPS2) is important for Sir2 and condensin recruitment. (A) Schematic diagram depicting the location of the DPS2 sequence deletion relative to other elements with the RE, with the deleted chromosome III coordinates indicated in red. **(B)** Quantitative ChIP of native Sir2 in WT and *dps2*Δ strains. **(C)** Quantitative ChIP of Brn1-Myc in WT and *dps2*Δ strains. *@RDT1* promoter indicates enrichment at the Sir2/condensin peak (**p<0.005).

Fig S4. Deleting the Sir2/condensin binding site within the RE (100bpΔ) does not alter Sir2 function at *HMLα*. (A) Quantitative mating assay for WT (ML1) and 100bpΔ (ML275) strains. **(B)** Quantitative ChIP assay showing Sir2 enrichment at *HML-I* in WT (ML1) and 100bpΔ (ML275) strains. (**p<0.005).

Fig S5. Auxin inducible degron (AID)-mediated depletion of Brn1 does not derepress *RDT1* or *HMLα*. (A) Western blot time course of auxin induced degradation of Brn1::V5-AID. Time indicates minutes after addition of auxin. **(B)** RT-qPCR of *RDT1* expression following 30 or 60 minutes of Brn1 depletion by auxin. **(C)** RT-qPCR of *HMLALPHA2* expression following 30 or 60 min of Brn1 depletion by auxin.

833 **Table S1. Genes closest to Sir2-dependent condensin peaks.** This Excel spreadsheet lists the
834 systematic ORF names of all genes that were closest to Sir2-dependent condensin peaks, as
835 chosen using MACS.
836
837 **Table S2. Yeast Strains.** List of all Saccharomyces cerevisiae strains used in this study, along
838 with their genotypes and source.
839
840 **Table S3. Oligonucleotides.** List of oligodeoxynucleotides used in this study.

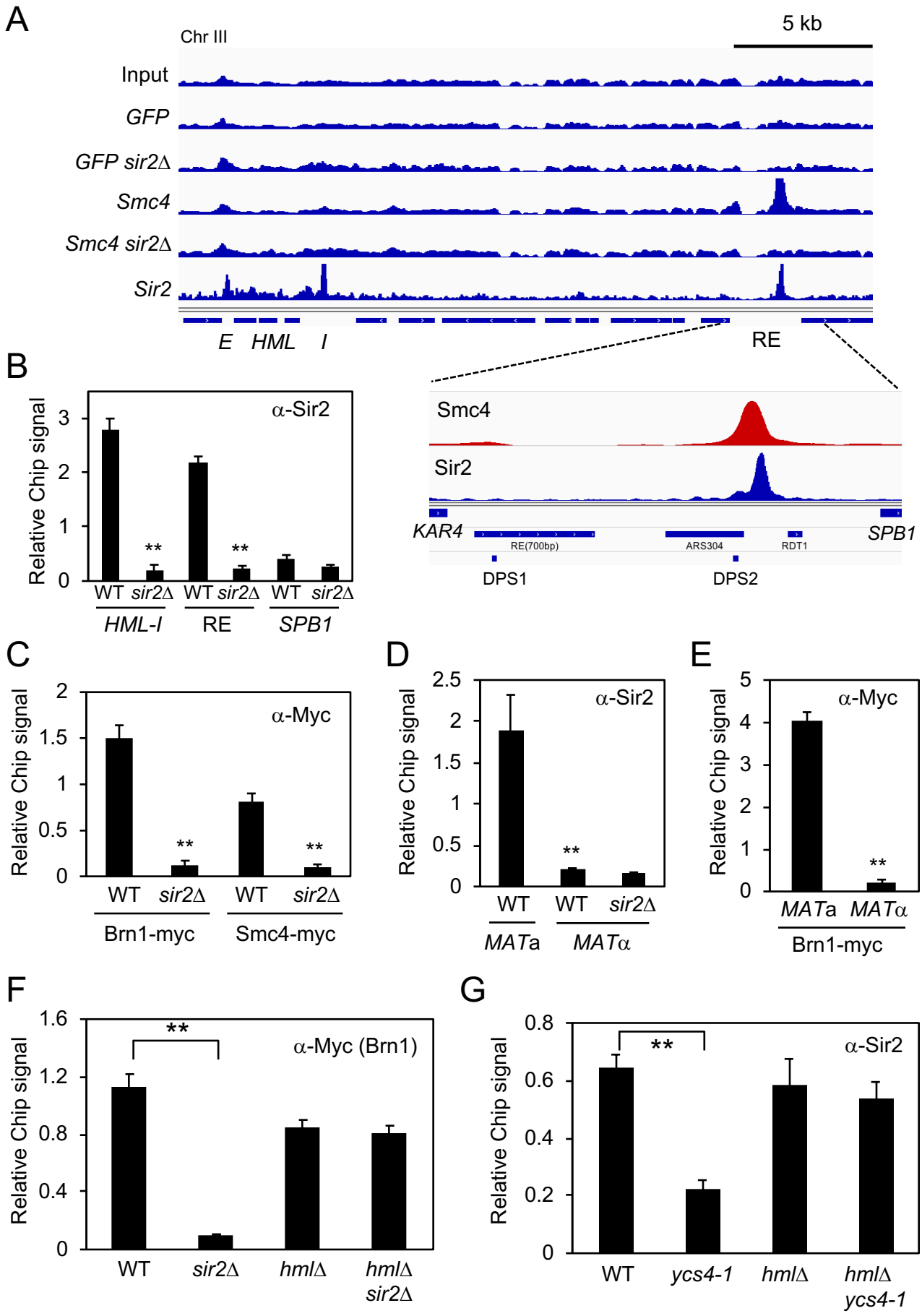
A
Chr III
5 kb
Input
GFP
GFP sir2Δ
Smc4
Smc4 sir2Δ
Sir2
E HML I
RE
B
Relative Chip signal
α-Sir2
WT sir2Δ WT sir2Δ WT sir2Δ
HML-I
RE
SPB1
Smc4
Sir2
KAR4
RE(700bp)
ARS304
RDT1
SPB1
DPS1
DPS2
C
Relative Chip signal
α-Myc
WT sir2Δ WT sir2Δ
Brn1-myc
Smc4-myc
D
Relative Chip signal
α-Sir2
WT WT sir2Δ
MATa
MATα
E
Relative Chip signal
α-Myc
MATa MATα
Brn1-myc
F
Relative Chip signal
α-Myc (Brn1)
WT
sir2Δ
hmlΔ
hmlΔ sir2Δ
G
Relative Chip signal
α-Sir2
WT
ycs4-1
hmlΔ
hmlΔ ycs4-1

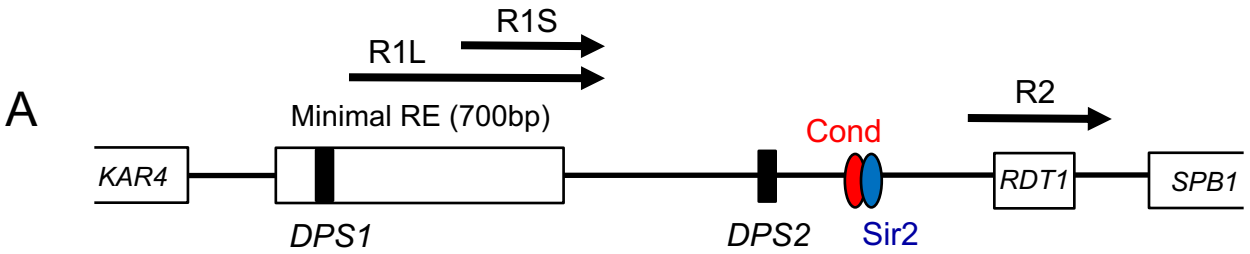
A
R1S
R1L
Minimal RE (700bp)
R2
Cond
KAR4
DPS1
DPS2
Sir2
RDT1
SPB1

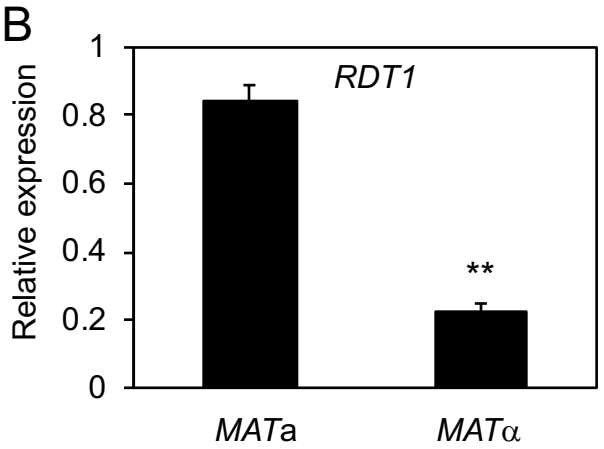
B
RDT1
Relative expression
1
0.8
0.6
0.4
0.2
0
**
MATa
MATα

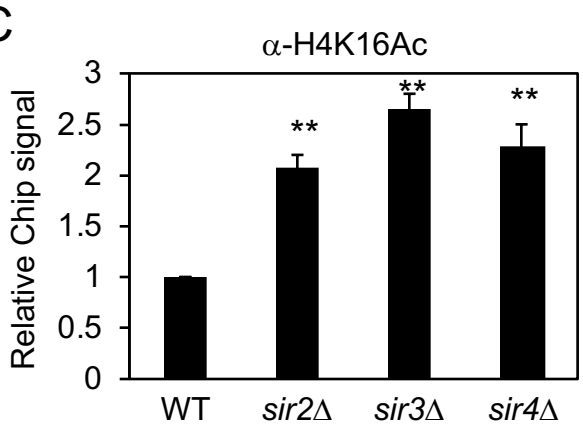
C
α-H4K16Ac
Relative Chip signal
3
2.5
2
1.5
1
0.5
0
**
**
**
WT
sir2Δ
sir3Δ
sir4Δ

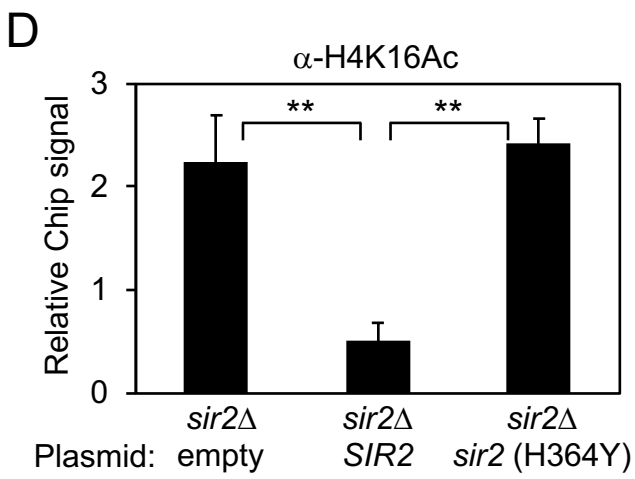
D
α-H4K16Ac
Relative Chip signal
3
2
1
0
**
**
sir2Δ
sir2Δ
sir2Δ
Plasmid: empty
SIR2
sir2 (H364Y)

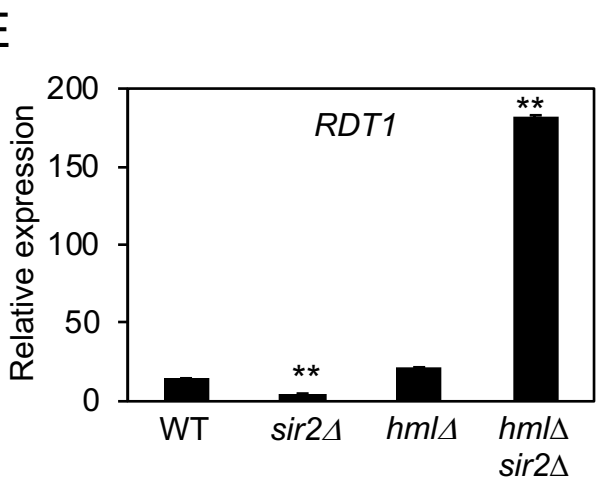
E
RDT1
Relative expression
200
150
100
50
0
**
**
WT
sir2Δ
hmlΔ
hmlΔ
sir2Δ

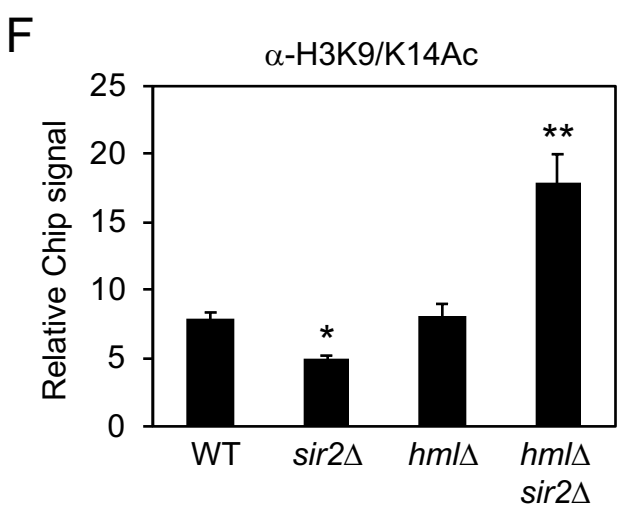
F
α-H3K9/K14Ac
Relative Chip signal
25
20
15
10
5
0
*
**
WT
sir2Δ
hmlΔ
hmlΔ
sir2Δ

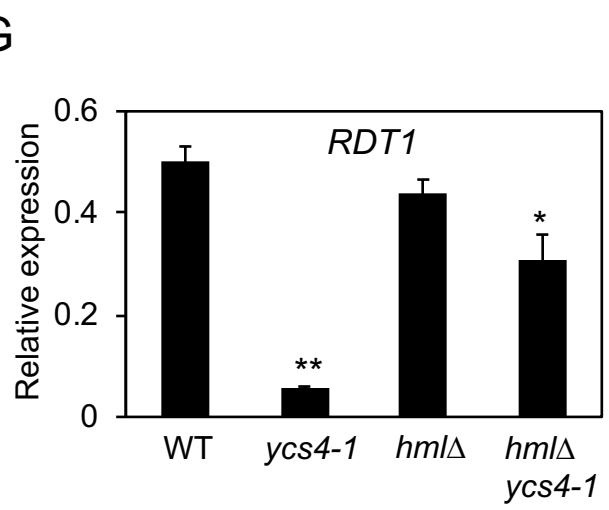
G
RDT1
Relative expression
0.6
0.4
0.2
0
**
*
WT
ycs4-1
hmlΔ
hmlΔ
ycs4-1

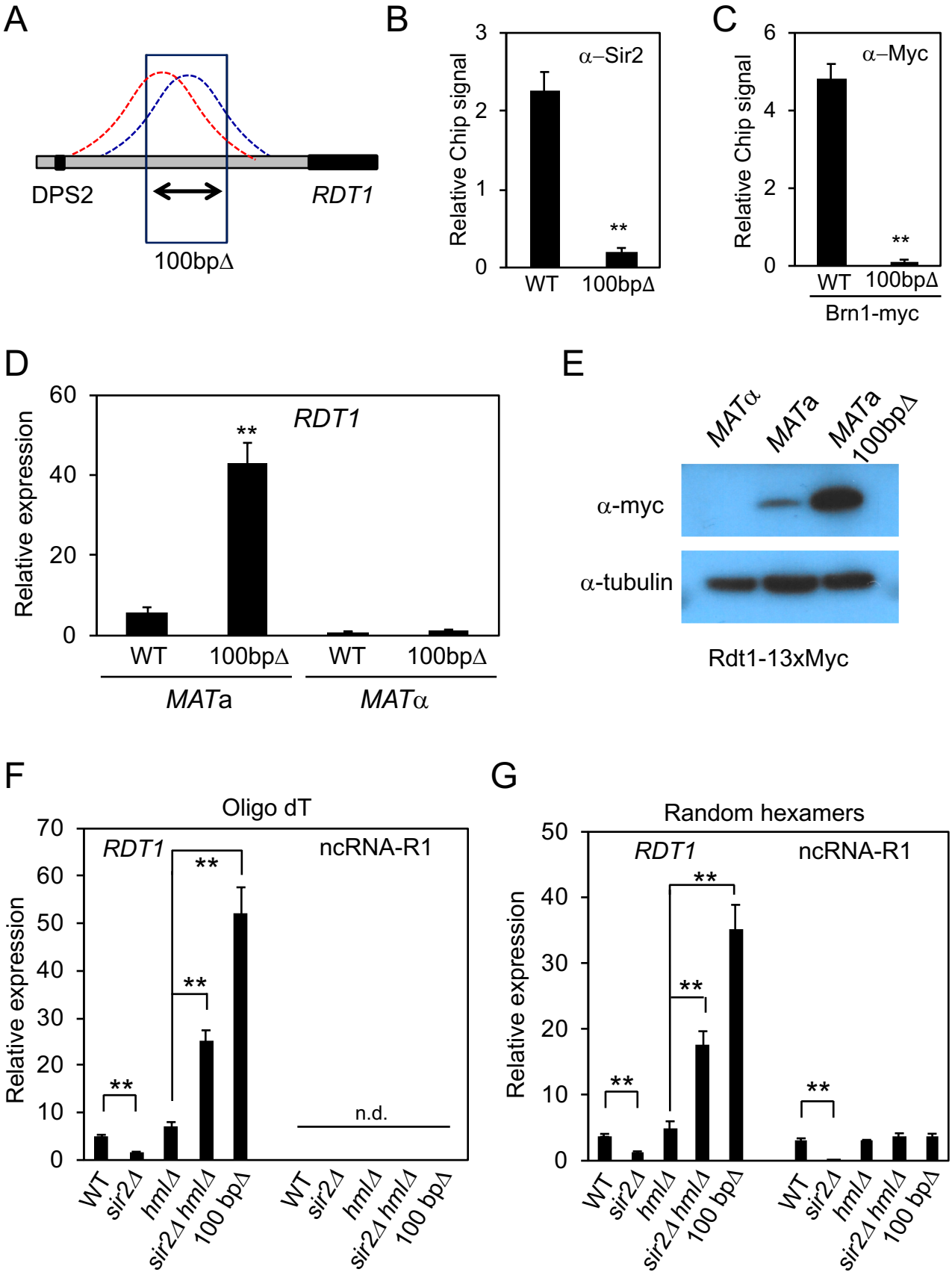
A
DPS2
RDT1
100bpΔ
B
α–Sir2
Relative Chip signal
WT
100bpΔ
C
α–Myc
Relative Chip signal
WT
100bpΔ
Brn1-myc
D
RDT1
Relative expression
WT
100bpΔ
WT
100bpΔ
MATa
MATα
E
MATα
MATa
MATa 100bpΔ
α-myc
α-tubulin
Rdt1-13xMyc
F
Oligo dT
RDT1
ncRNA-R1
Relative expression
n.d.
WT
sir2Δ
hmlΔ
sir2Δ hmlΔ
100 bpΔ
G
Random hexamers
RDT1
ncRNA-R1
Relative expression
WT
sir2Δ
hmlΔ
sir2Δ hmlΔ
100 bpΔ

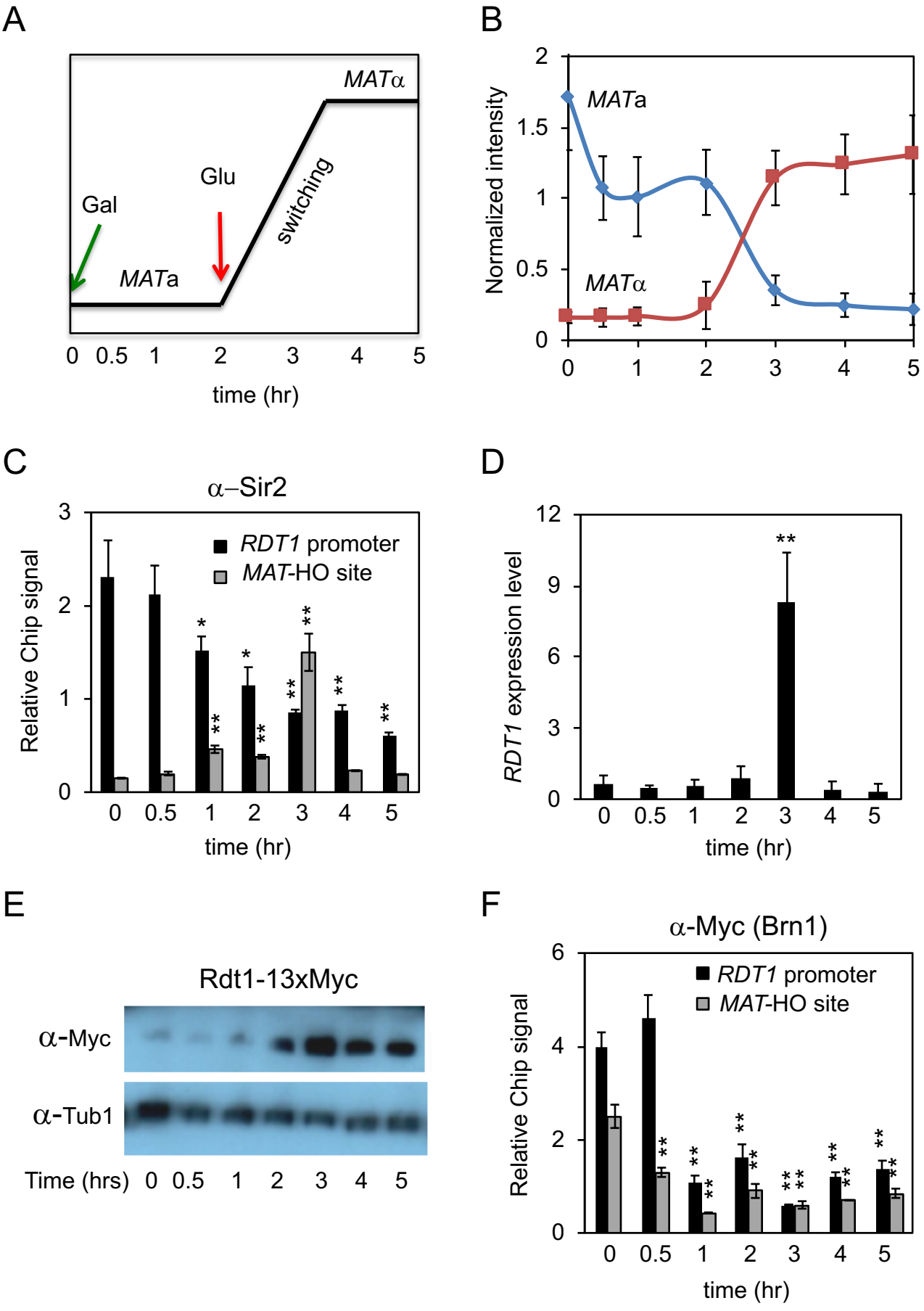
A
MATα
Glu
Gal
switching
MATa
0 0.5 1 2 3 4 5
time (hr)
B
Normalized intensity
MATa
MATα
0 0.5 1 1.5 2
0 1 2 3 4 5
C
α–Sir2
Relative Chip signal
RDT1 promoter
MAT-HO site
0 1 2 3
0 0.5 1 2 3 4 5
time (hr)
D
RDT1 expression level
0 3 6 9 12
0 0.5 1 2 3 4 5
time (hr)
E
Rdt1-13xMyc
α-Myc
α-Tub1
Time (hrs) 0 0.5 1 2 3 4 5
F
α-Myc (Brn1)
Relative Chip signal
RDT1 promoter
MAT-HO site
0 2 4 6
0 0.5 1 2 3 4 5
time (hr)

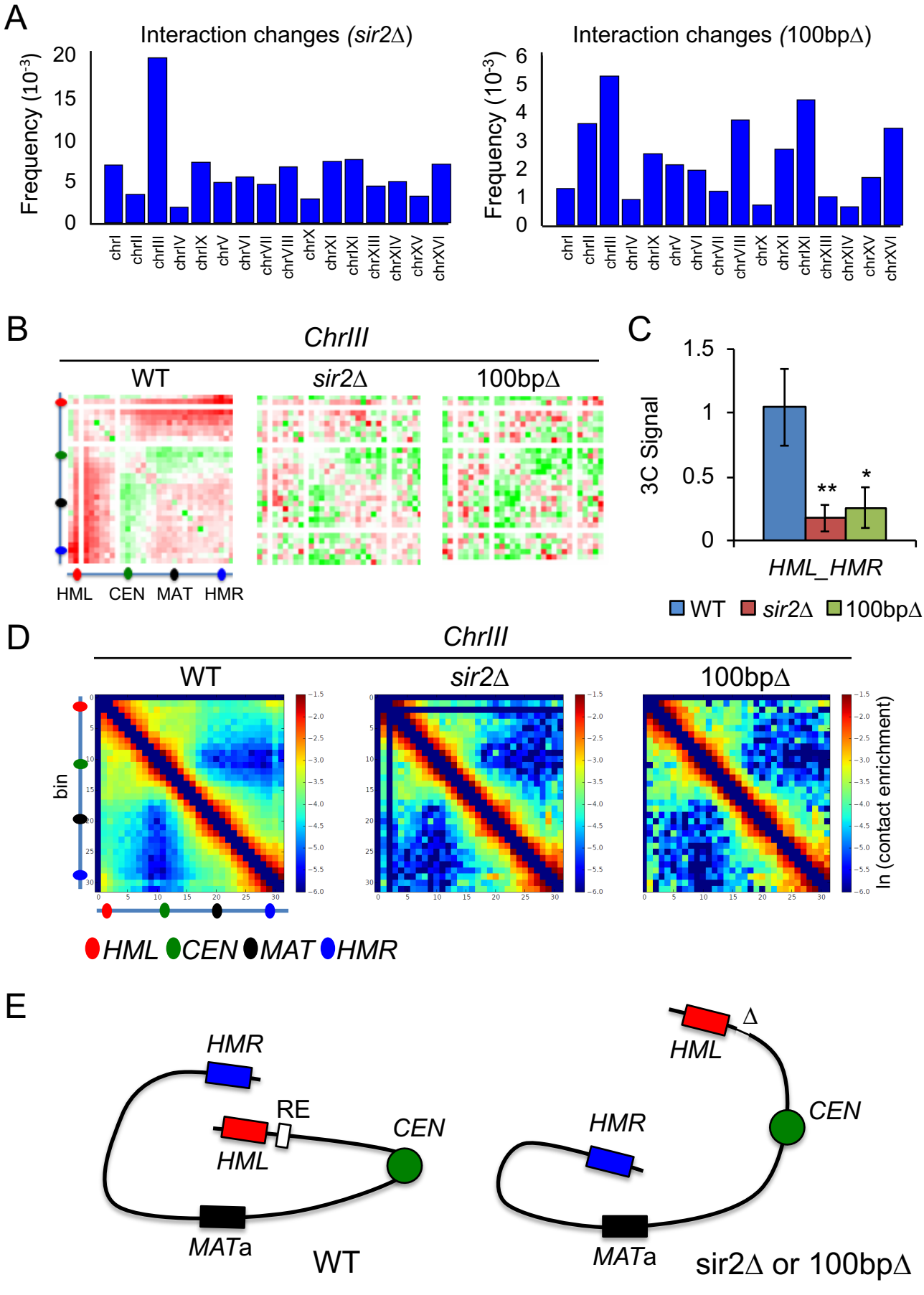
A
Interaction changes (sir2Δ)
Frequency (10-3)
20
15
10
5
0
chrI chrII chrIII chrIV chrIX chrV chrVI chrVII chrVIII chrX chrXI chrXII chrXIII chrXIV chrXV chrXVI
Interaction changes (100bpΔ)
Frequency (10-3)
6
5
4
3
2
1
0
chrI chrII chrIII chrIV chrIX chrV chrVI chrVII chrVIII chrX chrXI chrXII chrXIII chrXIV chrXV chrXVI
B
ChrIII
WT
sir2Δ
100bpΔ
HML CEN MAT HMR
C
3C Signal
1.5
1
0.5
0
**
*
HML_HMR
WT sir2Δ 100bpΔ
D
ChrIII
WT
sir2Δ
100bpΔ
bin
ln (contact enrichment)
HML CEN MAT HMR
E
HMR
RE
HML
CEN
MATa
WT
Δ
HML
HMR
CEN
MATa
sir2Δ or 100bpΔ

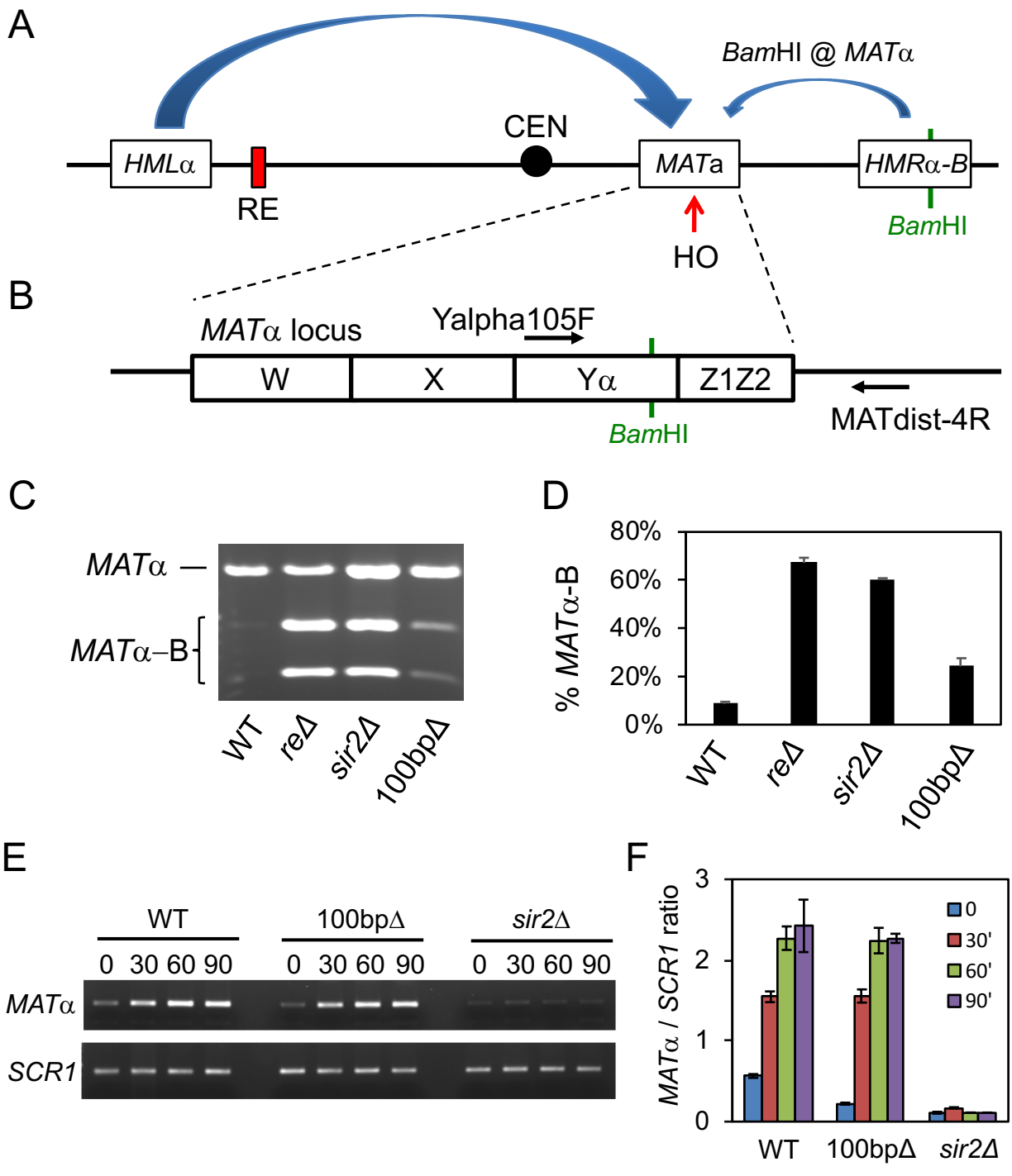
A
BamHI @ MATα
CEN
HMLα
RE
MATa
HMRα-B
BamHI
HO
B
MATα locus
Yalpha105F
W
X
Yα
Z1Z2
BamHI
MATdist-4R
C
MATα —
MATα–B
WT
reΔ
sir2Δ
100bpΔ
D
% MATα-B
80%
60%
40%
20%
0%
WT
reΔ
sir2Δ
100bpΔ
E
WT
100bpΔ
sir2Δ
0 30 60 90
0 30 60 90
0 30 60 90
MATα
SCR1
F
MATα / SCR1 ratio
3
2
1
0
0
30'
60'
90'
WT
100bpΔ
sir2Δ

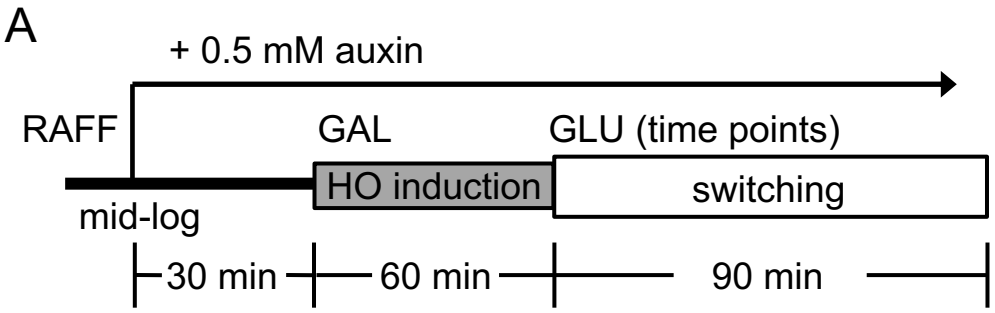
A
+ 0.5 mM auxin
RAFF
GAL
GLU (time points)
HO induction
switching
mid-log
30 min
60 min
90 min

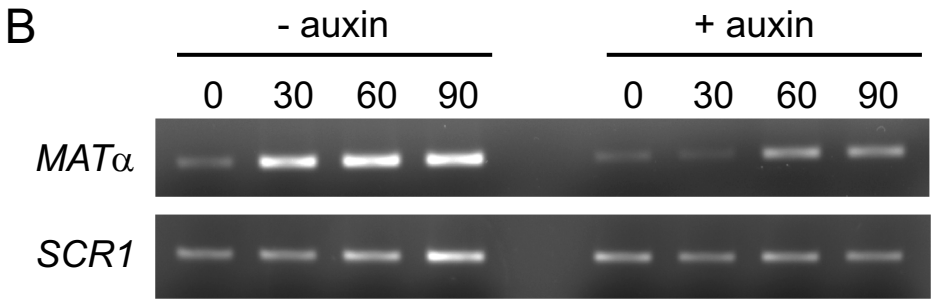
B
- auxin
+ auxin
0 30 60 90
0 30 60 90
MATα
SCR1

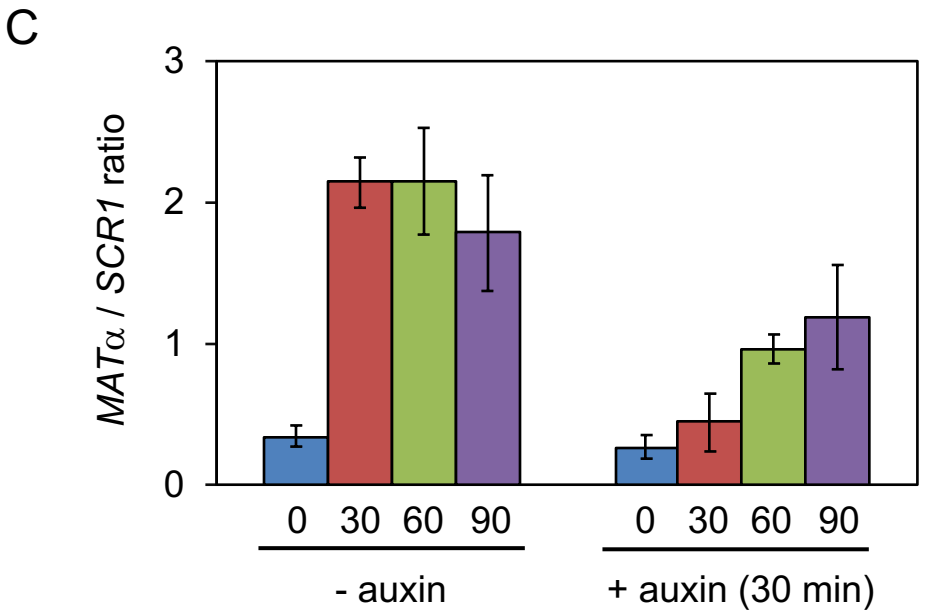
C
MATα / SCR1 ratio
3
2
1
0
0 30 60 90
0 30 60 90
- auxin
+ auxin (30 min)

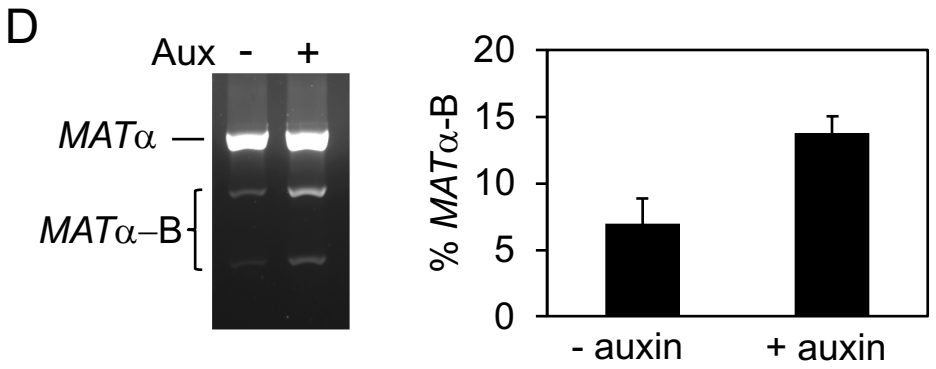
D
Aux - +
MATα
MATα–B
% MATα-B
20
15
10
5
0
- auxin
+ auxin